JOURNAL OF GEOPHYSICAL RESEARCH, VOL. 100, NO. A10, PAGES 19,135–19,145, OCTOBER 1, 1995

Magnetic fluctuations associated with tail current disruption: Fractal analysis

S. Ohtani,[1] T. Higuchi,[2] A. T. Y. Lui,[1] and K. Takahashi[3]

Abstract. The objective of the present study is to assess the mechanism of substorm-associated tail current disruption on the basis of magnetic field observations in the near-Earth tail. We examined 15 events observed by the Charge Composition Explorer (CCE) of the Active Magnetospheric Particle Tracer Explorers (AMPTE), with an emphasis on the August 28, 1986, event. In these events the satellite observed magnetic fluctuations to start almost simultaneously with ground substorm onsets, strongly suggesting that these fluctuations are related to the trigger of substorms. In this study we applied the new method, fractal analysis, to these fluctuations. This method enables us to examine fluctuations quantitatively and to pick up characteristic timescale(s) of fluctuations, even if fluctuations are far from sinusoidal. The results are summarized as follows: (1) Whereas before the onset of tail current disruption, magnetic fluctuations are suppressed in each of the magnetic components, after the onset, the magnitude of the H (north–south) component fluctuations is about 30% larger than the magnitudes of the fluctuations of the other components. (2) The magnetic fluctuations have a characteristic timescale, which is several times the proton gyroperiod. The first result suggests that observed magnetic fluctuations are actually related to changes in the tail current intensity, that is, tail current disruption. This result also indicates that the microprocess of tail current disruption should be described in terms of turbulent perturbation electric currents, although away from the onset region the effects of tail current disruption may be approximated by those of an orderly decrease in the tail current intensity. The second result strongly suggests that tail current disruption is driven by a certain instability, which grows most rapidly around that characteristic time scale, and in which ions should play an important role.

1. Introduction

In the near-Earth magnetotail a substorm onset is characterized by a change in the tail magnetic field from a stressed to a more dipolar configuration [e.g., *Cummings et al.*, 1968], which is often referred to as dipolarization. This phenomenon has been traditionally interpreted in terms of a decrease in the tail current intensity (tail current disruption). The associated current circuit, in which the disrupted current is converted into a pair of field-aligned currents with region 1 polarities, has been inferred to be responsible for the magnetosphere-ionosphere coupling during substorms [*Akasofu*, 1972; *McPherron et al.*, 1973; *Baumjohann et al.*, 1981].

The onset location of tail current disruption has been a central issue. The results of recent studies done from different viewpoints seem to be converging, strongly suggesting that tail current disruption initiates in the near-Earth region within 15 R_E from the Earth, possibly much closer to the Earth. Examples of such studies include (1) the observations of the onset of tail current disruption simultaneous with ground substorm onsets [*Takahashi et al.*, 1987; *Lui et al.*, 1988, 1992; *Lopez et al.*, 1990], (2) the timing studies of dipolarization signatures observed by multisatellite observations in the near-Earth tail [*Lopez et al.*, 1990; *Lopez and Lui*, 1990; *Ohtani et al.*, 1988, 1991], (3) the remote sensing of the tailward expansion of tail current disruption based on the variations of the lobe magnetic field [*Jacquey et al.*, 1991; *Ohtani et al.*, 1992], (4) the modeling of the buildup of the tail current intensity in the near-Earth tail [*Kaufmann*, 1987; *Pulkkinen et al.*, 1992], (5) the mapping of the auroral initial brightening to the equatorial plane [*Elphinstone et al.*, 1991], and (6) the formation of a substorm-associated field-aligned current system well equatorward of the open/close boundary [*Lopez et al.*, 1991].

Most of the previous studies focused on the macroscopic aspects of tail current disruption, such as the onset location, the spatial expansion, and relationships between magnetic and particle flux variations, principally because the spatial extent of the onset region is very limited [e.g., *Lopez and Lui*, 1990; *Ohtani et al.*, 1991, 1993]; therefore satellites usually observe the effects of tail current disruption away from the onset region. Thus, even though the concept of tail current disruption has been widely accepted, the trigger mechanism of tail current disruption is far from being completely understood (see recent review papers by *Lui* [1991] and *Fairfield* [1992]). This observational constraint led *Hesse and Birn* [1991] to an alternative interpretation of dipolarization signatures in terms of the pileup of magnetic fluxes ejected earthward from the near-Earth neutral line, which they have suggested forms further tailward of the synchronous region.

[1]The Johns Hopkins University Applied Physics Laboratory, Laurel, Maryland.
[2]The Institute of Statistical Mathematics, Tokyo, Japan.
[3]Solar Terrestrial Environment Laboratory, Nagoya University, Toyokawa, Japan.

Paper number 95JA00903.
0148-0227/95/95JA-00903$05.00

To verify the idea of tail current disruption and to understand its physical process, observations in the onset region are essential. Fortunately, data from the Charge Composition Explorer (CCE) of the Active Magnetospheric Particle Tracer Explorers (AMPTE) have provided such opportunities [*Takahashi et al.*, 1987; *Lui et al.*, 1988, 1992; *Lopez et al.*, 1990]. In fact, two previous studies [*Lui et al.*, 1992; *Burkhart et al.*, 1993] attempted to test their theoretical models by examining the power spectrum of onset-associated magnetic fluctuations. However, because of difficulties in the data analyses, at least two important problems remain to be answered. First, are such magnetic fluctuations actually related to changes in the tail current intensity? Second, do the fluctuations have characteristic timescales that may be associated with a certain instability? We believe that answers to these questions are important in understanding the mechanism of tail current disruption.

In this paper we apply a newly developed method for analyzing sequential data, fractal analysis [*Higuchi*, 1988, 1990], to magnetic fluctuations embedded in dipolarization signatures. This method has major advantages in quantifying fluctuations as well as in confirming or denying the existence of characteristic timescales. We explain the method in section 2. In section 3 we examine in detail an event observed by the AMPTE/CCE satellite on August 28 (day 240), 1986. Fourteen more events are examined in section 4. The results of the analysis are discussed in section 4. Section 5 summarizes the present study.

2. Analytical Method

The method that we adopted for the present study is characterized by the fact that it handles time series in the time domain rather than in the frequency domain. The method was originally proposed by *Higuchi* [1988] and was applied to measurements in various fields [e.g., *Bergamasco et al.*, 1990; *Yamamoto and Hughson*, 1993]. The theoretical evaluation was also made by *Theiler* [1991] and *Osborne and Provenzale* [1989].

The analytical procedure consists of two steps: (1) measuring the length $L(\tau)$ of time series $X(t) = X(j \cdot \Delta t)$ ($j = 1, 2, \ldots, N$; Δt: sampling interval) for different "scales" τ ($\tau = i \cdot \Delta t$; $i = 1, 2, 3, \ldots$), and (2) extracting necessary information from the dependence of $L(\tau)$ on τ. We will briefly outline each of the steps in the following. For details, see *Higuchi* [1988] and the other papers cited previously.

To calculate the length of $X(t)$ for τ, first we make k ($k = \tau/\Delta t$) subsets from $X(t)$:

$$X_{k,m}: X(m\Delta t), X(m\Delta t + \tau), X(m\Delta t + 2\tau), \ldots, X(m\Delta t + [(N-m)/k]\tau) \quad (m = 1, 2, \ldots, k) \tag{1}$$

where square brackets denote Gauss's notation; that is, $[a]$ indicates the largest integer that does not exceed a. The length of the mth subset $X_{k,m}$, $L_m(\tau)$, is defined as

$$L_m(\tau) = \left\{ \left(\sum_{i=1} \left| X(m\Delta t + i\tau) - X(m\Delta t + (i-1)\tau) \right| \right) A_m \right\} \Big/ \tau \tag{2}$$

The factor A_m ($= (N-1)/([(N-m)/k]k)$ is for adjusting the difference in the number of data points among the subsets. The length $L(\tau)$ is defined to be the average of $L_m(\tau)$ over the k subsets.

In equation (2) the term inside the braces is the summation of the absolute values of differences between two adjacent points separated by τ. Dividing this summation by τ in (2) is analogous to measuring the length of a line with compasses set at a certain distance. Assume that the curve is 10.0 cm long. For a compass width of 10 cm, the curve is measured to be 1, whereas for a compass width of 1 cm, the curve is measured to be 10. Thus the expression of the length depends on the setting of the compass. $L(\tau)$ is calculated for various values of τ ranging from the sampling interval Δt to a fraction of the total interval of the data set. Note that $L(\tau)$ is an increasing function of the number of data points; therefore it must be normalized to a certain interval when compared between intervals with different numbers of data points. In this study, $L(\tau)$ is normalized to 1 s; therefore, in the following, $L(\tau)$ is given in units of nT/s^2.

The next step is to examine the dependence of $L(\tau)$ on τ. If $L(\tau) \propto \tau^{-D}$, $X(t)$ is self-affine; D is referred to as fractal dimension. Such self-affine data have a power law spectrum $P(f) \propto f^{-\alpha}$ with $\alpha = 5 - 2D$ [*Mandelbrot*, 1977]; however, this conversion formula is not applicable for D values close to 1 and 2, which are the minimum and maximum values that D can take, respectively [*Higuchi*, 1990]. In some cases the logarithmic plot of $L(\tau)$ versus τ has a kink at a certain value of τ, τ_c. That is, the plot has different slopes in $\tau \leq \tau_c$ and $\tau_c \leq \tau$. This indicates that an associated physical process has a certain characteristic timescale T_c ($\neq \tau_c$; see the following discussion). It is expected that the corresponding power spectrum $P(f)$ also has a characteristic frequency f_c ($= 1/T_c$) and the power law index is different on the different sides of f_c. This expectation has been numerically confirmed by *Higuchi* [1990].

The relationship between T_c and τ_c was numerically examined by *Higuchi* [1989]. He applied fractal analysis to data sets which were numerically built so that their power spectrum has different slopes on different sides of $1/T_c$, α_L and α_H for $f < 1/T_c$ and $f > 1/T_c$. Then he surveyed the value of τ_c in the two-dimensional parameter space $\alpha_L - \alpha_H$. The result shows $T_c = 3$ to $5\tau_c$ (Figure 9 of *Higuchi* [1989]).

Figure 1 intuitively explains why τ_c is shorter than T_c. In this figure, $X(t)$ is assumed to be a sinusoidal wave with a period of T_c. Although, in fact, this assumption is an oversimplification from the viewpoint of the practical usage of the fractal analysis, the figure should also be helpful in understanding the outline of the analysis. As long as τ is sufficiently smaller than T_c (Figure 1a), we can trace each increase and decrease in $X(t)$ associated with the wave. Therefore the summation of the absolute values of differences between two adjacent points separated by τ does not depend on τ, and $L_m(\tau)$, and therefore $L(\tau)$, which is obtained by dividing the summation by τ, is inversely proportional to τ (see equation (2)). That is, the fractal dimension for the small timescale range is one. However, once τ becomes a fraction of T_c, the absolute value of the difference between two points separated by τ can take random values not exceeding the peak-to-peak amplitude of the wave and does not depend on τ. In this case, the summation is proportional to the number of data points ($\sim[N/k]$; see (1)) and is thus inversely proportional to τ. Therefore $L(\tau) \propto \tau^{-2}$; that is, the fractal dimension is two. Thus the power of $L(\tau)$ is different on the different sides of a certain value of τ, τ_c, which is shorter than T_c. It should also be noted that the fractal dimension of a one-dimensional data set ranges from one to two.

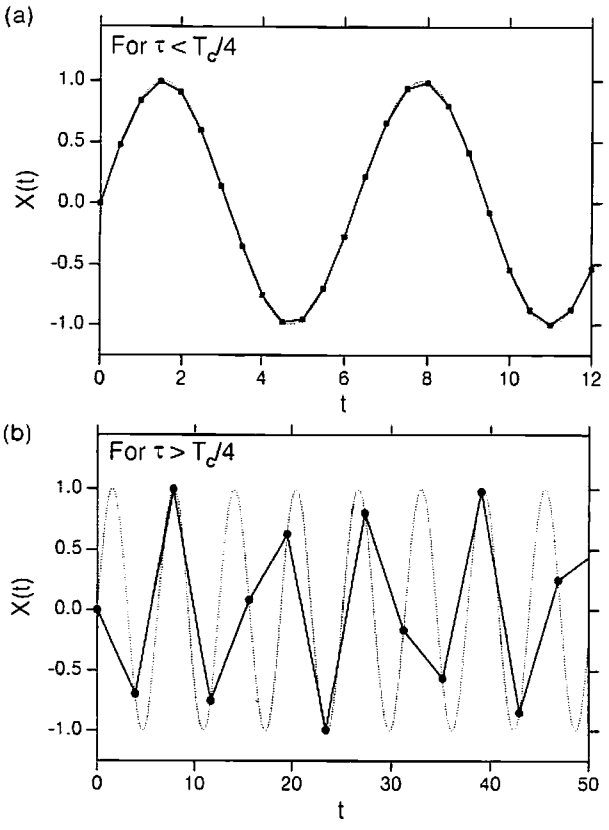

Figure 1. Schematic illustrations of the measurement of the length of fluctuations, $L(\tau)$, in cases in which τ is (a) significantly shorter than and (b) the significant fraction of the characteristic time scale (period) of fluctuations.

In the present analysis, τ_c is obtained by fitting two segments to the $\log(L(\tau))$ plot. Here, τ_c is determined so that the summation of the squares of differences between the plot and the segments is a minimum. The slopes of the segments, D_S and D_L for $\tau < \tau_c$ and $\tau_c < \tau$, respectively, represent fractal dimensions on each side of τ_c. The goodness of the two-segment fit is quantitatively evaluated by comparing the sum of squared residuals for the two-segment fit, σ_2^2, with that for the line fit, σ_1^2. There are cases where $\log(L(\tau))$ is better described by three, rather than two, segments with two characteristic timescales, τ_{cS} and τ_{cL}, for shorter and longer ones, respectively. As with the two-segment fit, we obtain τ_{cS} and τ_{cL} by least squares fit. The sum of the squared residual σ_3^2 is used as the goodness of fit.

The fast Fourier transform (FFT) is a reversible procedure, whereas the fractal analysis is not reversible but extracts information about the properties of fluctuations. The FFT provides characteristics of fluctuations in terms of frequencies and therefore may be more suitable for comparing observations with the results of theoretical studies, which often examine unstable Fourier components. However, fractal analysis has at least two major advantages.

First, the calculation of $L(\tau)$ is significantly more stable against abrupt phase changes of fluctuations than the calculation of a power spectrum, $P(f)$. Note that in the calculation of $L(\tau)$ the effects of phase changes are localized around each of the changes. On the other hand, such phase changes affect the total integration/summation of the Fourier transform. Second, the fractal analysis works even for fluctuations whose characteristic timescale is a significant fraction of the interval of data sets. Since in the Fourier analysis $P(f)$ is calculated for discrete values of f separated equally ($\Delta f = (N\Delta t)^{-1}$, where N is the total number of data points), we do not have many data points in a low-frequency range. On the other hand, the fractal analysis has no methodological restriction in selecting values of t, although the calculation of $L(\tau)$ is less stable for τ closer to the whole duration of the data interval. Since the region of tail current disruption is spatially localized, the spacecraft does not remain in the disruption region for very long, and the dynamics of a current sheet cause rapid motion of the spacecraft relative to the spatial structure of signatures, resulting in abrupt changes in the phase of magnetic fluctuations. Thus these two points are crucial in examining current disruption.

3. Case Study: August 28, 1986, Event

3.1. Outline of the Event

An event we selected for a case study occurred on August 28 (day 240), 1986. This event provides a unique opportunity, because the AMPTE/CCE satellite was in the disruption region at a substorm onset and remained in the region for as long as 3 min. The event was originally reported by *Takahashi et al.* [1987] and was examined later by *Lui et al.* [1992] and *Burkhart et al.* [1993] from different viewpoints.

Figure 2 shows a 20-min (1145–1205) plot of the AMPTE/CCE magnetometer data sampled every 0.124 s (see *Potemra*

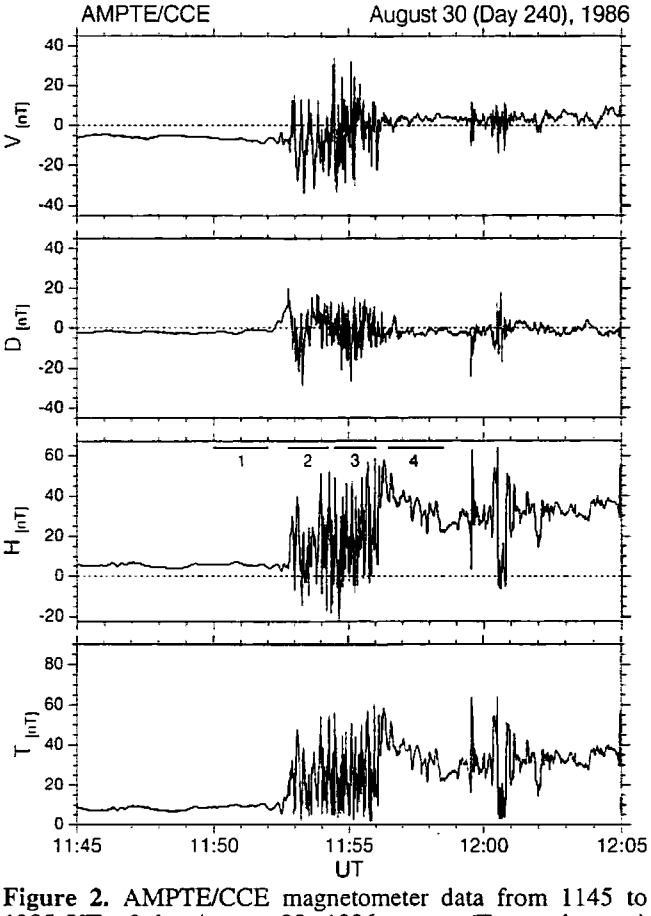

Figure 2. AMPTE/CCE magnetometer data from 1145 to 1205 UT of the August 28, 1986, event. (Top to bottom) The V, D, and H magnetic components and the total field strength. The horizontal bars in the H component panel represent the intervals we selected for the fractal analysis.

et al. [1985] for details of the instrument). The satellite was in the midnight local time sector, MLT = 23.5, at a radial distance of approximately $8R_E$. The data are shown in V, D, and H coordinates. In this coordinate system, H is antiparallel to the dipole axis, V points radially outward and is parallel to the magnetic equator, and D completes a right-hand orthogonal system (positive eastward). A 19.75-s time offset was discovered in the CCE data after *Takahashi et al.* [1987] published their paper, and this offset was corrected in Figure 2.

Each magnetic component started to change irregularly at 1152:30 UT, following a quiet interval. The highly irregular fluctuations continued for several minutes. The H component increased in the course of the fluctuations, indicating that the tail magnetic field changed from a stretched to a more dipolar configuration. Energetic ion fluxes also increased in association with this configurational change of the magnetic field (not shown; see Figure 1 of *Takahashi et al.* [1987] and Plate 2 of *Lui et al.* [1992]). A ground substorm activity was confirmed by a Pi 2 onset observed at Kakioka at 1154 (±1 min) UT [*Takahashi et al.*, 1987]. The CCE event started several tens of seconds earlier than the Pi 2 onset. This time delay may be attributed to the Alfvén transit time. The most striking feature of Figure 2 is that the H component repeatedly made negative (southward) excursions. Also, the sign of the V component altered frequently, indicating that the satellite was very close to the neutral sheet; the magnetic latitude of the spacecraft position was −2.4° at 1200 UT. From the timing and the magnetic signatures, we infer that the AMPTE/CCE spacecraft was located in the onset region and remained in the region for as long as 3 min. Thus this event provides an ideal opportunity for examining magnetic fluctuations associated with tail current disruption.

Figure 3 expands the 5-min interval of 1152–1157 UT. The properties of magnetic fluctuations are different before and after 1154 UT. Short-timescale fluctuations are obviously more intense for the latter period. Referring to Figures 2 and 3, we selected the following four intervals for the analysis; each interval is marked by a horizontal bar in the panel of the H component plots of Figures 2 and 3.

Interval 1	1150:00–1152:00 UT	ΔT = 120 s (N = 966 points)
Interval 2	1152:45–1154:15 UT	ΔT = 90 s (N = 725 points)
Interval 3	1154:30–1156:00 UT	ΔT = 90 s (N = 725 points)
Interval 4	1156:30–1158:30 UT	ΔT = 120 s (N = 967 points)

Interval 1 is before the onset. Intervals 2 and 3 are during the early and late phases of highly irregular magnetic fluctuations, respectively. Each magnetic component became relatively stable after the sudden jump of the H component at about 1156:05 UT. Interval 4 is selected from such a period.

3.2. Comparison with FFT

We selected the H component of interval 2 for the comparison between the present analysis and the conventional FFT; the reason for this selection is that the interval is just after the onset, and also that the H component is inferred to be most closely related to changes in the tail current, as discussed later. The top panel of Figure 4 plots $L(\tau)$ versus τ in the logarithmic scale, whereas the bottom panel shows the power spectrum $P(f)$. Note that in the top panel, the timescale (τ) is longer toward the right of the horizontal axis. In the bottom panel the

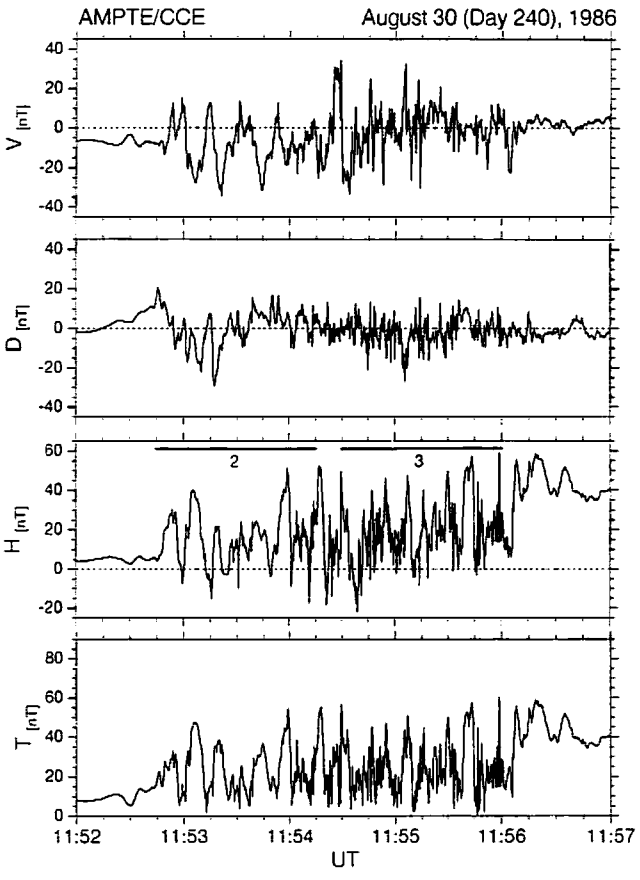

Figure 3. Expanded plot of the AMPTE/CCE magnetometer data from 1152 to 1157 UT.

horizontal axis represents the frequency, and therefore the timescale is longer toward the left.

The plot of $L(\tau)$ is very smooth (top panel). The dotted lines in the top panel represent the results of the two-segment fit (see section 2). The fit is successful. The slope of $L(\tau)$ obviously changes at τ_c = 4.0 s, indicating that the fluctuations have a characteristic time. (We confirmed that the method adopted by *Theiler* [1991] gives a very similar value of τ_c.) The corresponding "period" T_c ($3\tau_c$~$5\tau_c$; see section 2) is inferred to be 12 s < T_c < 20 s. (The characteristic timescale of fluctuations will be discussed later in more detail.) The slope of the fitted line, which corresponds to the fractal dimension, is 1.3 for $\tau < \tau_c$ and 2.2 for $\tau > \tau_c$. Theoretically, the dimension of one-dimensional sequential data should not exceed 2.0. Presumably, this discrepancy arises from difficulties in calculating $L(\tau)$ for longer time scales. Note that the duration of the interval is 90 s, and each value of $L_m(\tau)$ is calculated on the basis of a limited number of data points at $\tau > \tau_c$; the maximum value of τ is 16 s for the present case (section 2).

In contrast to the plot of $L(\tau)$, many irregular fluctuations are embedded into the power spectrum (Figure 4b). The vertical segments in the panel mark $1/(3\tau_c)$ and $1/(5\tau_c)$, where τ_c = 4 s, determined by the two-segment fit in the fractal analysis. It is expected that the power spectrum has a kink in this range of f. However, it is difficult to specify its location, although the plot of $P(f)$ probably has two slopes. This is because we have a very limited number of spectral estimates in the low-frequency range, as marked by open circles. In the higher-frequency range, the spectrum is well approximated by $f^{-2.4}$, cor-

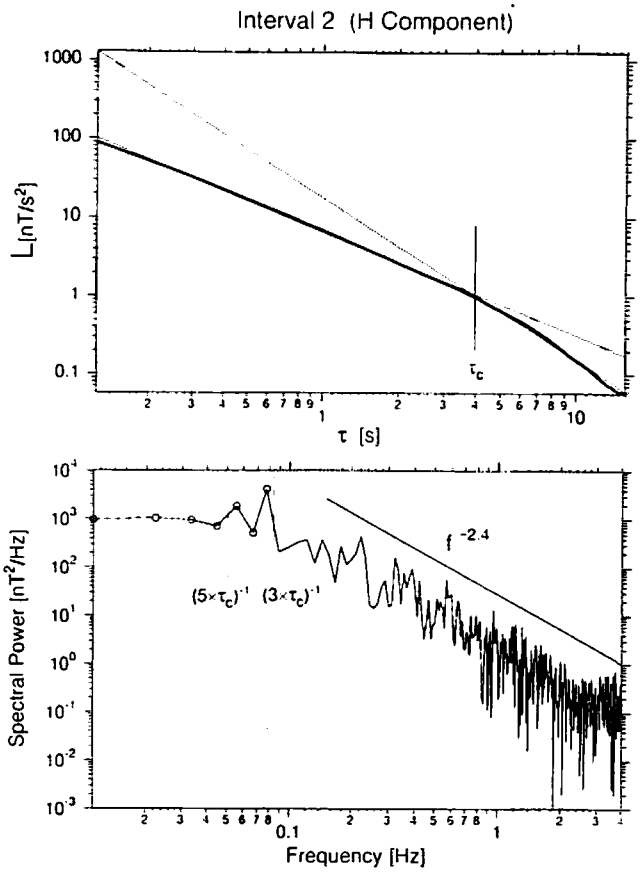

Figure 4. Comparison of the (top) fractal and (bottom) Fourier analyses for the H component during interval 2, from 1152:45 to 1154:15 UT. The dotted lines in the top panel show the results of the two-segment fitting.

responding to the fractal dimension, 1.3, for $\tau < \tau_c$ ($\alpha = 5 - 2D$; D is the fractal dimension). On the other hand, the plot seems to be almost flat at $f < 1/(5\tau_c)$, giving α close to zero. The disagreement from the estimate of α based on $\alpha = 5 - 2D$, which gives $\alpha = 1$ for $D = 2$, is ascribed to the limited applicable range of this conversion formula [*Higuchi*, 1990; see also section 2].

3.3. Results of the Fractal Analysis

Figure 5 plots $L(\tau)$ versus τ in the logarithmic scale for the three magnetic components (V, D, and H) and the total field strength for the four intervals. Note that the vertical scale is different from panel to panel. Figure 6 compares the $\tau - L(\tau)$ plots of the H component for the four intervals.

Before the onset (interval 1; Figure 5a), fluctuations are suppressed, and the kink of the $L(\tau)$ plot is not evident in any component. The comparison between the intervals before the onset (interval 1) and after (interval 2; Figure 5b) reveals that $L(\tau)$ of each component increased by a factor of several tens (see also Figure 6). For interval 2, the H component fluctuations have a characteristic timescale at $\tau_c = 4.0$ s, corresponding to 12 s $< T_c <$ 20 s, as mentioned previously. The proton gyroperiod based on the average magnetic field strength during (before) the interval, T_G ($T_{G(\text{preonset})}$), is 2.8 s (6.8 s). Therefore the characteristic time scale of the H component fluctuation is several (a few) times longer than T_G ($T_{G(\text{preonset})}$). A kink is also found in the plots of the V and D components. As determined by the least squares fit, τ_c is 3.0 s for the V component and 2.1 s for the D component. The difference in τ_c among the components may reflect different kinds of electric currents, that is, cross-tail currents and field-aligned currents, which flow in different directions and have different spatial structures, and therefore result in perturbations in different magnetic components. The difference may result also from spacecraft motion relative to the spatial structure of perturbation currents, which affects different magnetic components differently.

Interval 3 is distinguished from interval 2 by enhancement in short timescale fluctuations (Figure 3). The comparison of the H component between intervals 2 and 3 (Figure 6) indicates that $L(\tau)$ increased primarily in a short-timescale range, and the two plots do not differ significantly in a long-period range. This is true also for the other components. A three-segment curve rather than a two-segment curve represented $L(t)$ of the H component well; $\sigma_2^2/\sigma_3^2 = 4.3$ (section 2). The two characteristic timescales determined are $\tau_{cS} = 1.1$ s and $\tau_{cL} = 7.2$ s. The corresponding periods, T_{cS} and T_{cL}, are 3.3 s $< T_{cS} <$ 5.5 s and 21.6 s $< T_{cL} <$ 36.0 s for τ_{cS} and τ_{cL}, respectively. The proton gyroperiod T_G for this interval is 2.7 s. Thus T_{cS} is close to T_G, whereas T_{cL} is longer than T_G by almost an order of magnitude. The $L(\tau)$ plots of the V and D components for interval 3 are represented by two-segment curves, rather than three-segment curves, and both components have τ_c at 1.1 s, which is the same as τ_{cS} of the H component. This fact suggests that the short-period fluctuations are dominant in the V and D components.

During interval 4, $L(\tau)$ is smaller than during interval 3 by an order of magnitude (Figures 5 and 6). This result is expected from the plots of the magnetometer data, which show that each component is less irregular during interval 4. Obviously, the $L(\tau)$ plot of the H component has a kink, which is at $\tau_c = 5.9$ s (Figure 5d). Although $L(\tau)$ of the H component is larger than the other two components in the whole range of τ, the difference is largest at 3 s $< \tau <$ 10 s. This can be seen also in Figure 2. Long timescale fluctuations (of the order of a few tens of seconds) remain in the H component, whereas in the other two components both long and short timescale fluctuations are suppressed. The proton gyroperiod for this interval is 1.9 s. Again, the characteristic period T_c, which is $3\tau_c < T_c < 5\tau_c$, is significantly longer than the proton gyroperiod. However, for this interval, we need to be careful in comparing T_c (or τ_c) with the gyroperiod. Note that the magnetic field is persistently directed northward, and the H component is several times as large as the preonset level. Therefore it is likely that the observed magnetic signatures are the effects of current disruption taking place away from the spacecraft.

3.4. Temporal Variations of $L(\tau)$

In closing this section, let us compare $L(t)$ among the three magnetic components. As shown in Figure 5, whereas before the onset (interval 1) the fluctuation is largest in the V component, followed by the H component, the order is reversed during interval 2, except in a long-period range of τ, 9 $s < \tau <$ 14 s (Figure 5b). The H component fluctuations are largest also for intervals 3 and 4 (Figures 5c and 5d).

To examine the variations of the characteristics of fluctuations in the course of the event, we calculated $L(\tau)$ for a 1-min period centered every 30 s. Figure 7 compares the sequences of $L(\tau_{\min})$ ($\tau_{\min}$: sampling interval, 0.124 s) of the three magnetic

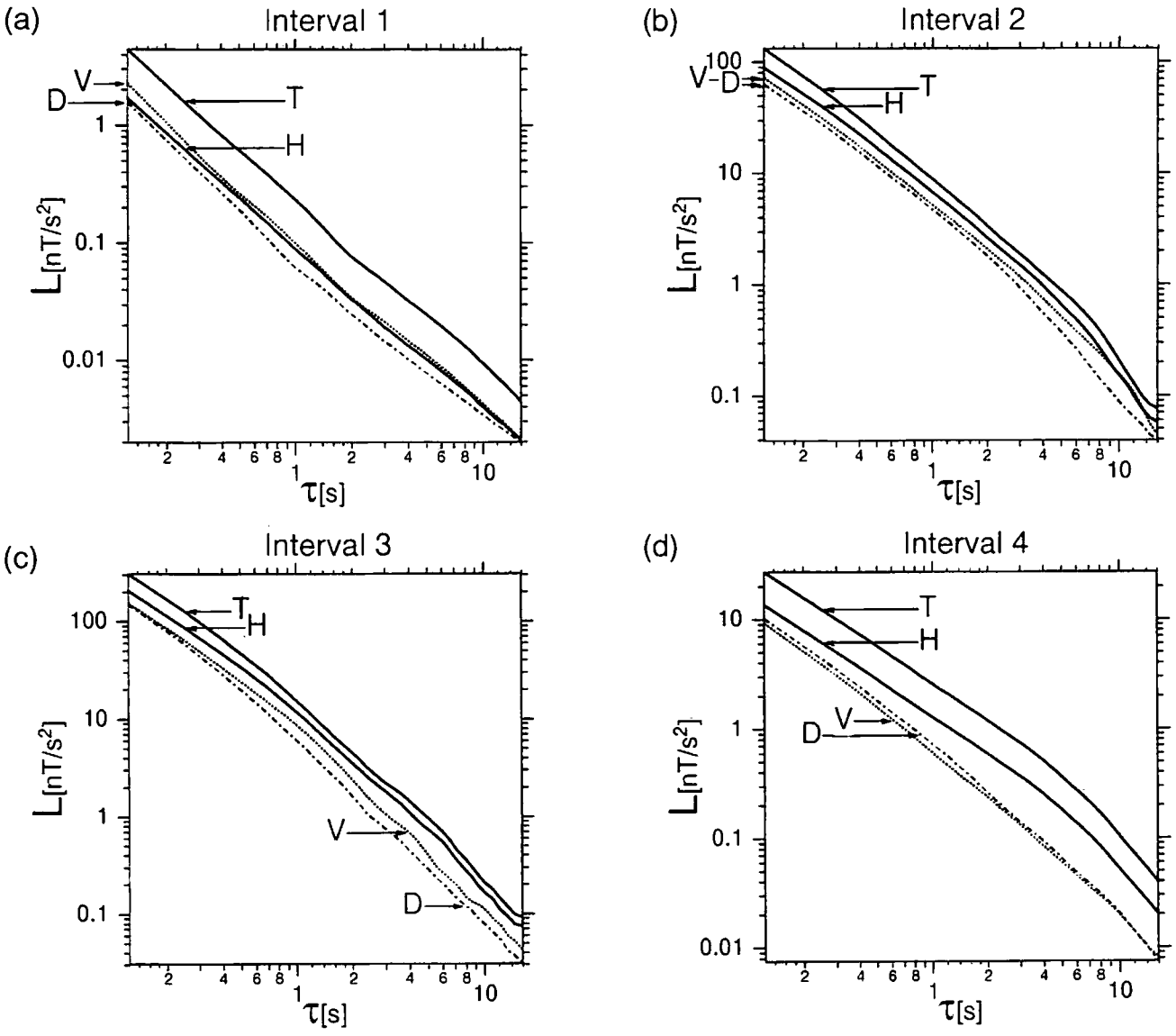

Figure 5. $L(\tau)$ versus τ in the logarithmic scale for the three magnetic components (V, D, and H) and the total field strength for the four intervals: (a) interval 1; 1150:00–1152:00 UT, (b) interval 2; 1152:45–1154:15 UT, (c) interval 3; 1154:30–1156:00 UT, and (d) interval 4; 1156:30–1158:30 UT.

components, denoted by different symbols. The insert expands the period before the onset, which shows that $L(\tau_{min})$ is largest for the V component before the onset. On the other hand, throughout the period of current disruption, $L(\tau_{min})$ is largest for the H component (the solid circles), followed by the V component (the open circles), until 1155 UT. The difference between the D (the open triangles) and V components is not significant afterward. These facts are all consistent with Figure 5. Differences in $L(\tau)$ among the components should be informative on a current system associated with the magnetic fluctuations and will be discussed later.

4. Statistical Study

In the previous section we applied the fractal analysis to substorm-associated magnetic fluctuations observed by the AMPTE/CCE spacecraft in the August 28, 1986, event. *Lui et al.* [1992] surveyed the AMPTE/CCE data during the period of April 1985 to November 1986 and found 15 such events; the August 28 event is one of them. Each of the events was observed within a few minutes from a ground substorm onset observed in the same local time sector as the spacecraft. In this section we examine these 15 events by focusing on the characteristic timescale and amplitude of magnetic fluctuations.

Table 1 lists the 15 events; the August 28 event is event 8. The UTs indicate intervals for which we applied the fractal analysis. These intervals were selected by visually examining the plots of the magnetic field data so that the properties of the fluctuations and the background magnetic field do not change during each of the intervals. The duration of the intervals ranges from 75 to 180 s. A proton gyroperiod (T_G) is calculated on the basis of the average field strength during each of the intervals.

Figure 8 shows $L(\tau_{min})$ (τ_{min} = 0.124 s) of the three magnetic components for before (Figure 8a) and after (Figure 8b) onsets. The intervals before onsets were also selected by visu-

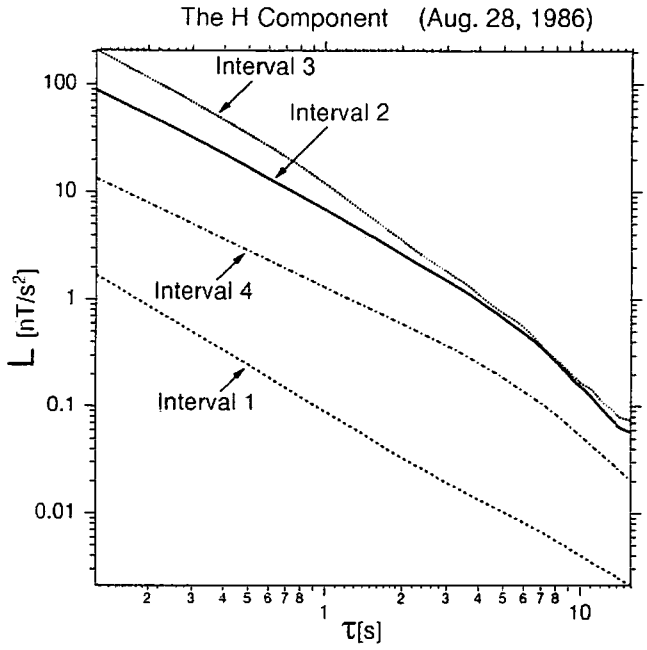

Figure 6. Superposition of the plots of $L(\tau)$ of the H component for the four intervals.

ally examining the plots of the magnetic field data. Note that the vertical scales are different between the two panels; the ratio of $L(\tau_{min})$ after to before onsets is typically a few tens. We used the same preonset values for event 9 as for event 8 because this event started at 1200 UT on August 28, immediately after event 8 (Figure 2). Before onsets the V-component fluctuations are largest, except for event 15. This result might be due to the vertical (Z direction) motion of the spacecraft relative to the current layer; the V component is most sensitive to such a motion. On the other hand, after onsets (Figure 8b), fluctuations are largest in the H component, as we found for event 8 in section 3, except for events 3 and 10. In these events, $L(\tau_{min})$ is largest for the V component, although the differences between the V and H components are not significant and can barely be recognized in the figure. The average ratios of the amplitude of the H component to those of the V and D components are both 1.3.

Next, let us examine τ_c (= 1/5~1/3T_c) of magnetic fluctuations. We focus on the H component. The reason for this is twofold. First, as just shown, the fluctuations are largest in the H component after onsets in almost all events. Second, in contrast to the H component, the other two components (V and D) should be sensitive to the spacecraft distance from the neutral sheet, and therefore magnetic fluctuations associated with the substorm onset process in these components are not easily distinguished from fluctuations caused by the motion of the current layer, which is inferred to be most active after onsets.

A characteristic timescale was found to exist for each of the events, as shown in Table 1. Each value of τ_c was determined by the least squares method (section 2) and was also confirmed by visually examining the $L(\tau)$ versus τ plot. (The values of σ_1^2/σ_2^2 range from 3.0 to 33.5, with an average of 12.9.) For events 7 and 13, the three-segment fit was found to describe the $L(\tau)$ plot better than the two-segment fit; $\sigma_2^2/\sigma_3^2 > 4$ (section 2). The fractal dimension obtained for $\tau < \tau_c$, D_S, takes almost the same value, ~1.3, in all events. For events 8 and 11, the fractal dimension for $\tau > \tau_c$, D_L (also the fractal dimension for $\tau > \tau_{cL}$ for event 13), exceeds two, which is theoretically impossible and is presumably due to difficulties in calculating $L(\tau)$ for long timescales. The average value of D_L is 1.8; we assumed that D_L is two for events 8 and 11. The fractal dimensions of 1.3 and 1.8 correspond to power law indices of 2.4 and 1.4, respectively, for the power spectrum.

Figure 9 shows τ_c of the H component fluctuations normalized by proton gyroperiods. In Figure 9a a proton gyroperiod, T_G, was calculated on the basis of the average magnetic field strength during the interval of fluctuations. However, the amplitude of the magnetic fluctuations is usually as large as the background field strength, and therefore the average magnetic field strength during the fluctuations may not be a good reference. For this reason, in Figure 9b, τ_c is normalized by a proton gyroperiod ($T_{G(preonset)}$), calculated on the basis of the magnetic field strength before an onset. For event 9 we used the same preonset field strength as for event 8. For events 7 and 13, both τ_{cS} (the open triangles) and τ_{cL} (the open circles) are plotted. The horizontal dotted line in Figure 9a (Figure 9b) represents τ_c/T_G ($\tau_c/T_{G(preonset)}$) = 1/3. Note that almost all points are above these lines; exceptions are event 1 in the top panel and event 5 in Figure 9b. The average of τ_c/T_G ($\tau_c/T_{G(preonset)}$) is 1.7 (1.1); here we excluded cases where $L(\tau)$ has two characteristic timescales. Thus the characteristic timescale, T_c (= 3~5τ_c), is several times the proton gyroperiod, not depending on the definition of the proton gyroperiod.

5. Discussion

In previous sections we examined magnetic fluctuations observed in the near-Earth tail in association with a substorm onset. The results are summarized as follows: (1) The amplitude of magnetic fluctuations is largest for the H component. (2) The magnetic fluctuations do have a characteristic timescale, which is several times the proton gyroperiod. In this section we discuss each of these two major results.

5.1. Current System Associated with the Magnetic Fluctuations

The first result indicates that electric currents associated with the magnetic fluctuations tend to flow parallel to the cur-

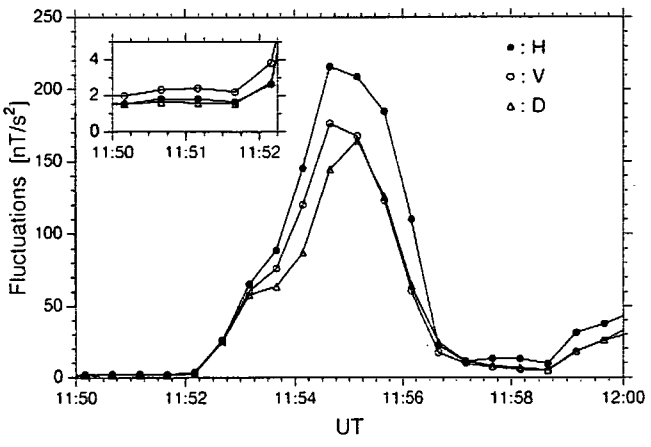

Figure 7. Comparison of $L(\tau_{min})$ of the three magnetic components in the course of the event. The insert expands a preonset period.

Table 1. List of Events With Spacecraft Position and Results of the Fractal Analysis

Number	Year	DOY	Date	Time, UT	R, R_E	MLT, Hours	dZ, R_E	T_G, s	$\tau_c(H)$, s	D_S	D_M	D_L
1	1985	115	Apr. 25	0111:40–0112:20	8.6	1.4	−0.02	4.68	1.4	1.3		1.6
2	1985	133	May 13	2111:30–2114:00	7.5	23.9	−0.62	1.55	2.4	1.3		1.8
3	1985	152	Jun. 1	2121:30–2123:00	8.6	23.7	−0.19	2.98	7.2	1.2		1.8
4	1985	152	Jun. 1	2314:00–2315:30	8.8	0.3	0.22	3.59	14.5	1.3		1.8
5	1985	158	Jun. 7	2209:00–2210:30	8.2	0.6	−0.27	2.55	1.1	1.4		1.6
6	1985	163	Jun. 12	0950:30–0953:30	8.8	23.3	0.31	3.63	3.6	1.2		1.6
7	1986	234	Aug. 22	1601:30–1604:00	8.5	0.2	−0.40	3.12	(1.5, 14.5)	1.2	1.5	1.9
8	1986	240	Aug. 28	1152:45–1154:15	8.1	23.4	0.03	2.79	4.0	1.3		2.1
9	1986	240	Aug. 28	1200:00–1202:00	8.1	23.5	0.02	2.15	6.6	1.3		1.8
10	1986	242	Aug. 30	0948:20–0949:40	7.4	22.9	0.48	1.97	4.7	1.3		1.9
11	1986	242	Aug. 30	1223:45–1225:00	8.7	23.9	0.07	2.99	5.6	1.3		2.2
12	1986	243	Aug. 31	2006:20–2007:45	8.8	0.2	−0.36	3.52	2.4	1.2		1.6
13	1986	248	Sept. 5	0916:30–0919:00	8.7	23.6	0.89	1.83	(2.7, 17.2)	1.2	1.5	2.3
14	1986	292	Oct. 19	2211:45–2213:00	7.7	23.1	0.12	2.30	1.2	1.2		1.5
15	1986	320	Nov. 16	0447:00–0450:00	8.8	20.7	0.14	3.13	6.6	1.4		2.0

R, radial distance; dZ, distance from the neutral sheet.

rent sheet (equatorial plane). Note that if currents tend to flow in the vertical (north-south) direction, the fluctuations should be largest in the V or D component, instead of the H component. However, it should be emphasized that the amplitude of the H component fluctuation is larger than, but does not overwhelm, the amplitudes of the fluctuations of the other components. Although to some extent the V and D component fluctuations may be explained in terms of the motion of the spacecraft relative to the structures of cross-tail currents and field-aligned currents, it is improbable to completely ascribe the V and D component fluctuations to such spatial effects. This is so because in most cases the peak-to-peak amplitudes of the V and D component fluctuations are significantly larger than the levels after the fluctuations (see Figure 2), indicating that rather large spatial displacement is necessary for explaining the fluctuations. It

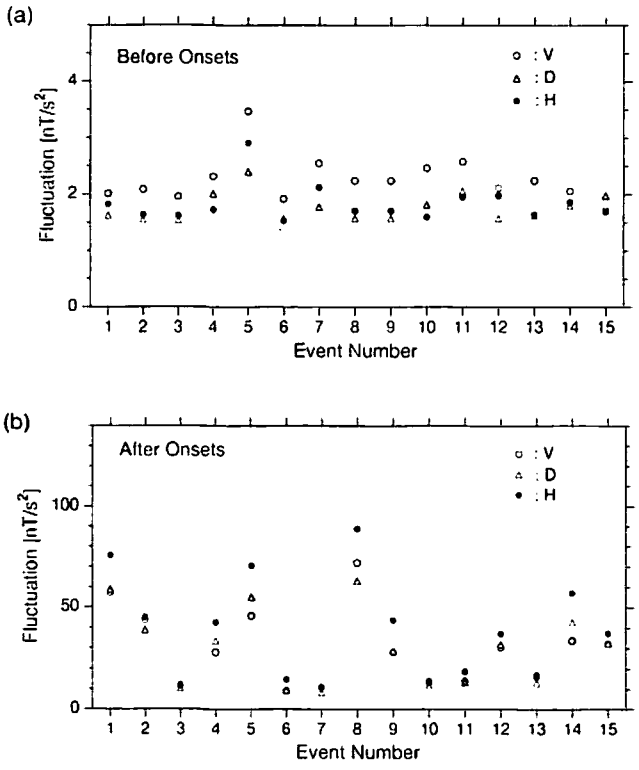

Figure 8. $L(\tau_{min})$ (τ_{min} = 0.124 s) of the three magnetic components for (a) before and (b) after onsets of the 15 events listed in Table 1. The event number corresponds to that of Table 1. The vertical scales are different between the two panels.

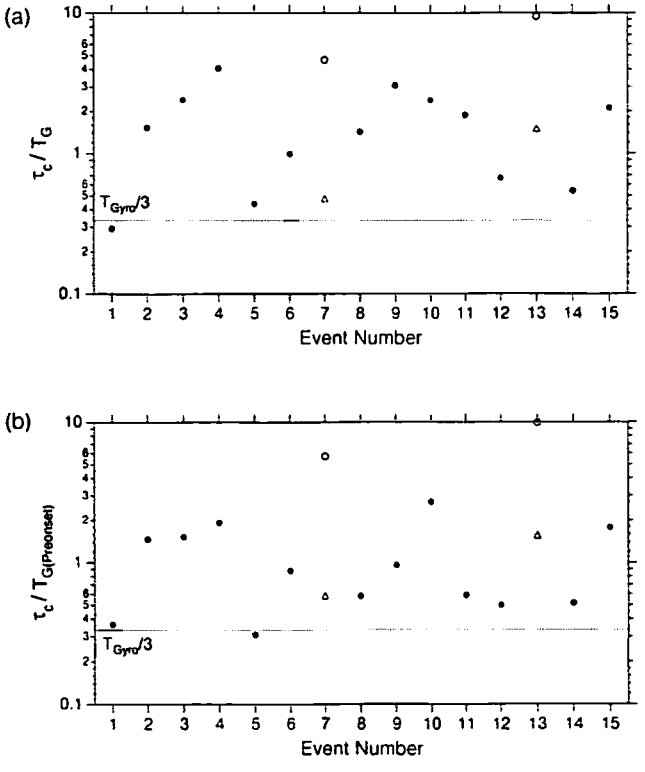

Figure 9. Characteristic timescales τ_c of the H component fluctuations for the 15 events listed in Table 1. The solid circles indicate the results of the two-segment fit, and the open circles and open triangles indicate those of the three-segment fit for cases $\sigma_2^2/\sigma_3^2 > 4$. In the top panel, τ_c is normalized by a proton gyroperiod calculated on the basis of the average magnetic field strength during the same interval of the fluctuations, whereas in the bottom panel, τ_c is normalized by a proton gyroperiod calculated on the basis of the preonset magnetic field strength. The horizontal dashed line in the top (bottom) panel represents $\tau_c/T_G(\tau_c/T_{G(\text{preonset})}) = 1/3$.

is unlikely that such a dynamic motion of the current layer has a characteristic timescale as short as several times the ion gyroperiod (result 2).

Therefore, so far as perturbation electric currents are concerned, the magnetic fluctuations may be envisioned as being caused by filamentary currents that flow in various directions, but preferentially parallel to the neutral sheet. However, the present result does not put any constraint on the average direction of such filamentary currents. For example, a positive variation of the H component can be caused by a line current flowing in the dusk-to-dawn direction on the tailward side of the satellite, but also by a line current flowing in the opposite direction on the earthward side of the satellite. In fact, there are infinite possibilities about the direction of a current that causes a positive H variation at the satellite position. Note that even if we use the three components, this ambiguity cannot be eliminated.

On the other hand, it seems very reasonable to infer that the observed magnetic fluctuations are caused by local changes in electric currents, not by changes occurring far away from the satellite. Considering that at geosynchronous altitude a substorm onset is characterized by an increase in the H component (note that all events we examined took place outside the geosynchronous orbit), we infer that such filamentary currents are actually related to changes in the cross-tail current intensity. Away from the disruption region the effects of such filamentary currents are almost averaged out, and resultant magnetic signatures, which are often called dipolarization, are well described in terms of the decrease in the tail current intensity.

One may think that the magnetic fluctuations observed in association with substorm onsets are ion cyclotron waves excited locally due to injected particles, which probably have a perpendicular temperature higher than a parallel temperature. However, this possibility can be excluded by result 1. The linear kinetic theory indicates that the ion cyclotron instability has maximum growth at parallel propagation, for which an excited wave is not compressible [*Gary*, 1992]. On the other hand, in the events that we examined, the spacecraft was located very close to the neutral sheet, where the H component is the major component of the background magnetic field. Therefore the largest magnitude of the H component fluctuations is not consistent with the idea that the fluctuations are excited by the ion cyclotron instability. It should also be useful to comment on the anisotropy of ion fluxes observed in the August 28 event (Plate 2 of *Lui et al.* [1992]). For interval 2, the interval just after the onset, the distribution of energetic ions was rather isotropic, which is not favorable for the ion cyclotron instability. On the other hand, the pancake distribution of ions observed during interval 3 might be responsible for the enhancement in the intensity of shorter timescale fluctuations.

5.2. Substorm Trigger Models

The second result should be important in understanding the mechanism of tail current disruption. The existence of a characteristic timescale in the magnetic fluctuations strongly suggests that tail current disruption is driven by a certain instability, which grows fastest around that characteristic timescale. Since the characteristic timescale is several times the proton gyroperiod, it is inferred that the dynamics of ions are important in the instability. In the following paragraphs, on the basis of the present results, we will make a brief comment on several models that are suggested to be responsible for the substorm process in the near-Earth tail (see *Lui* [1991] and *Fairfield* [1992] for recent reviews of substorm trigger models).

The tearing mode instability has been an attractive candidate for a trigger mechanism. *Schindler* [1974] proposed that ions are unmagnetized near the neutral sheet before a substorm onset because the field line curvature becomes comparable to their Larmor radius, and such ions destabilize the (ion) tearing mode. The importance of the behavior of ions, which this model proposes, is consistent with the present results. However, the instability strongly depends on the behavior of electrons, such as pitch angle scattering by waves [*Pellat et al.*, 1991; *Kuznetsova and Zelenyi*, 1991] and nonadiabatic stochastic diffusion [e.g., *Büchner and Zelenyi*, 1989]. The question of the ion tearing mode instability remains very controversial.

Lui et al. [1991] applied a cross-field current instability to the inner edge of the cross-tail current just prior to the onset of tail current disruption by adopting plasma parameters observed during that time by the CCE spacecraft. For the ion drift speed equal to half the ion thermal speed, they found that the current sheet is unstable to a broad spectrum of oblique whistler waves in the frequency range of $0.02f_g$ to $0.4f_g$ (f_g is the proton gyrofrequency), implying characteristic timescales of 2 to 50 times the proton gyroperiod. The real frequency of unstable modes increases, and therefore the characteristic timescale decreases, with a higher relative drift speed between ions and electrons. The growth rates of the unstable waves in this frequency range are within a factor of 2 of each other (see their Figure 6). Therefore the characteristic timescales obtained from this study are in good agreement with the predicted unstable wave frequencies from the cross-field current instability.

The ballooning instability is also a considerable, but a controversial, possibility as a substorm trigger mechanism [*Roux et al.*, 1991; *Lee and Wolf*, 1992; *Ohtani and Tamao*, 1993]. This instability has been traditionally regarded as an MHD instability, and the microscale behavior of ions has not been taken into account except in a very few papers such as the one by *Chen and Hasegawa* [1991], which examined this instability in the context of magnetic pulsations. Considering that the characteristic timescale is several times the proton gyroperiod, we suggest that future applications of this instability to a substorm trigger mechanism also need to include kinetic effects.

The thermal catastrophe model [*Smith et al.*, 1986; *Goertz and Smith*, 1989] proposes that the Alfvén resonance in the plasma sheet boundary layer provides a source of energy for triggering substorms. There is a difficulty in interpreting the fluctuations examined in this study in terms of the (kinetic) Alfvén wave associated with this model. That is, the satellite remained close to the neutral sheet during the events, whereas the model predicts that the wave decays equatorward of the resonant layer.

Kan et al. [1988] have proposed that a substorm is triggered directly by the ionospheric response to an enhanced magnetospheric convection during the growth phase. The characteristic timescale associated with the magnetosphere-ionosphere (M-I) coupling is inferred to be an Alfvén bounce period, which is of the same order as that of Pi 2 pulsations, 40 to 150 s. Thus the characteristic timescale of the magnetic fluctuations observed by AMPTE/CCE is significantly shorter than the time scale of the M-I coupling. Although this fact does not exclude a possibility that the M-I coupling controls conditions for triggering current disruption, the trigger instability of tail current disruption should be a local process, rather than a global one such as M-I coupling.

5.3. Remaining Problems

At least two questions remain before the mechanism of current disruption can be identified. The first question is whether the behavior of ions is adiabatic or nonadiabatic, in other words, whether ions move freely across the magnetic field. Although the characteristic timescale is longer than the proton gyroperiod, this does not necessarily mean that ions behave adiabatically. The reason for this is twofold. First, fluctuations also exist in a range of timescales much shorter than this characteristic timescale (see Figure 4). Second, the magnetic configuration is also an important factor in determining the motions of particles [e.g., *Büchner and Zelenyi*, 1989]; the motion of ions becomes nonadiabatic when the thickness of the tail current sheet becomes comparable to the Larmor radius.

The second question is how important heavy ions are in the instability. The important role of O^+ ions in triggering substorms has been proposed on the basis of both theories [e.g, *Baker et al.*, 1985] and observations [e.g., *Daglis et al.*, 1994]. The gyroperiod of O^+ ions is longer than the proton gyroperiod, and is close to or longer than the characteristic timescale of the magnetic fluctuations. Such heavy ions may behave differently from protons and may make a major contribution to tail current disruption, although the O^+ contribution to the energy density is rather low (see Table 3 of *Lui et al.* [1992] or Figure 11 of *Daglis et al.* [1994]).

6. Summary

In this study we have quantitatively examined the magnetic fluctuations observed by AMPTE/CCE in the near-Earth tail. We applied the new analytical method, fractal analysis, to 15 events previously reported [*Takahashi et al.*, 1987; *Lui et al.*, 1992], with an emphasis on the August 28, 1986, event. We found that after the substorm onset, the H component (north-south) fluctuations are 30% larger than the fluctuations of the other (V and D) components. This fact indicates that electric currents associated with the magnetic fluctuations flow in various directions, but preferentially parallel to the equatorial plane. Considering that the tail field typically changes to a more dipolar configuration at a substorm onset at geosynchronous altitude, earthward of the AMPTE/CCE events, we infer that these fluctuations are actually related to tail current disruption. We also found that the magnetic fluctuations have a characteristic timescale, which is several times the proton gyroperiod, implying that ions play an important role in disrupting a tail current. The range of the characteristic timescale is in good agreement with that of the unstable modes of the cross-field current instability. Although further work is necessary to uniquely determine the trigger mechanism of tail current disruption, we believe that the results of the present study place an important constraint on future studies of modeling substorm initiation.

Acknowledgments. We are very grateful to T. A. Potemra, L. J. Zanetti, and the Space Department of The Johns Hopkins University Applied Physics Laboratory (JHU/APL) for making the AMPTE/CCE magnetometer data available for this study. This work was supported by the Atmospheric Sciences Section of the National Science Foundation, grant ATM-9114316 to JHU/APL. Work at APL was also supported by NASA and the Office of Naval Research.

The Editor thanks L. Bergamasco for her assistance in evaluating this paper.

References

Akasofu, S.-I., Magnetospheric substorms: A model, in *Solar Terrestrial Physics*, part 3, pp. 131–151, edited by Dyer, D. Reidel, Norwell, Mass., 1972.

Baker, D. N., E. W. Hones Jr., D. T. Young, and J. Birn, The possible role of ionospheric oxygen in the initiation and development of plasma sheet instabilities, *Geophys. Res. Lett.*, *9*, 1337, 1982.

Baker, D. N., T. A. Fritz, R. L. McPherron, D. H. Fairfield, Y. Kamide, and W. Baumjohann, Magnetotail energy storage and release during the CDAW 6 substorm analysis intervals, *J. Geophys. Res.*, *90*, 1205, 1985.

Baumjohann, W., R. J. Pellinen, H. J. Opgenoorth, and E. Nielsen, Joint two-dimensional observations of ground magnetic and ionospheric electric fields associated with auroral zone currents: Current systems associated with local auroral break-ups, *Planet. Space Sci.*, *29*, 431, 1981.

Bergamasco, L., A. Provenzale, G. C. Castagnoli, M. Serio, V. A. Kudrjavtsev, V. A. Kuznetsov, and O. G. Ryazhskaya, Effects of the solar cycle on the fractal and statistical properties of deep underground muons, *J. Geophys. Res.*, *95*, 2419–2425, 1990.

Büchner, J., and L. M. Zelenyi, Regular and chaotic charged particle motion in magnetotaillike field reversals, 1, Basic theory of trapped motion, *J. Geophys. Res.*, *94*, 11,821, 1989.

Burkhart, G. R., P. B. Dusenbery, T. W. Speiser, and R. E. Lopez, Hybrid simulations of thin current sheets, *J. Geophys. Res.*, *98*, 21,373, 1993.

Chen, L., and A. Hasegawa, Kinetic theory of geomagnetic pulsations, 1, Internal excitations by energetic particles, *J. Geophys. Res.*, *96*, 1503, 1991.

Cummings, W. D., J. N. Barfield, and J. P. Coleman Jr., Magnetospheric substorms observed at the synchronous orbit, *J. Geophys. Res.*, *73*, 6887, 1968.

Daglis, I. A., S. Livi, E. T. Sarris, and B. Wilken, Energy density of ionospheric and solar wind origin ions in the near-Earth magnetotail during substorms, *J. Geophys. Res.*, *99*, 5691, 1994.

Elphinstone, R. D., D. Hearn, J. S. Murphree, and L. L. Cogger, Mapping using the Tsyganenko long magnetospheric model and its relationship to Viking auroral images, *J. Geophys. Res.*, *96*, 1467, 1991.

Fairfield, D. H., Advances in magnetospheric storm and substorm research: 1989–1991, *J. Geophys. Res.*, *97*, 10,865, 1992.

Gary, S. P., The mirror and ion cyclotron anisotropy instabilities, *J. Geophys. Res.*, *97*, 8519, 1992.

Goertz, C. K., and R. A. Smith, The thermal catastrophe model of substorms, *J. Geophys. Res.*, *94*, 6581, 1989.

Hesse, M., and J. Birn, On dipolarization and its relation to the substorm current wedge, *J. Geophys. Res.*, *96*, 19,417, 1991.

Higuchi, T., Approach to an irregular time series on the basis of the fractal theory, *Physica D*, *31*, 277, 1988.

Higuchi, T., Fractal analysis of time series (in Japanese), *Proc. Inst. Stat. Math.* *37*, 209, 1989.

Higuchi, T., Relationship between the fractal dimension and the power law index for a time series: A numerical investigation, *Physica D*, *46*, 254, 1990.

Jacquey, C., J. A. Sauvaud, and J. Dandouras, Location and propagation of the magnetotail current disruption during substorm expansion: Analysis and simulation of an ISEE multi-onset event, *Geophys. Res. Lett.*, *18*, 389, 1991.

Kan, J. R., L. Zhu, and S.-I. Akasofu, A theory of substorms: Onset and subsidence, *J. Geophys. Res.*, *93*, 5624, 1988.

Kaufmann, R. L., Substorm currents: Growth phase and onset, *J. Geophys. Res.*, *92*, 7471, 1987.

Kuznetsova, M. M., and L. M. Zelenyi, Magnetic reconnection in collisionless field reversals: The universality of the ion tearing mode, *Geophys. Res. Lett.*, *18*, 1825, 1991.

Lee, D.-Y., and R. A. Wolf, Is the Earth's magnetotail balloon unstable?, *J. Geophys. Res.*, *97*, 19,251, 1992.

Lopez, R. E., and A. T. Y. Lui, A multisatellite case study of the expansion of a substorm current wedge in the near-Earth magnetotail, *J. Geophys. Res.*, *95*, 8009, 1990.

Lopez, R. E., H. Lühr, B. J. Anderson, P. T. Newell, and R. W. McEntire, Multipoint observations of a small substorm, *J. Geophys. Res.*, *95*, 18,897, 1990.

Lopez, R. E., H. E. Spence, and C.-I. Meng, DMSP F7 observations of a substorm field-aligned current, *J. Geophys. Res.*, *96*, 19,409, 1991.

Lui, A. T. Y., A synthesis of magnetospheric substorm models, *J. Geophys. Res.*, *96*, 1849, 1991.

Lui, A. T. Y., R. E. Lopez, S. M. Krimigis, R. W. McEntire, L. J. Zanetti, and T. A. Potemra, A case study of magnetotail current sheet disruption and diversion, *Geophys. Res. Lett.*, 15, 721, 1988.

Lui, A. T. Y., C.-L. Chang, A. Mankofsky, H.-K. Wong, and D. Winske, A cross-field current instability for substorm expansions, *J. Geophys. Res.*, *96*, 11,389, 1991.

Lui, A. T. Y., R. E. Lopez, B. J. Anderson, K. Takahashi, L. J. Zanetti, R. W. McEntire, T. A. Potemra, D. M. Klumpar, E. M. Greene, and R. Strangeway, Current disruptions in the near-Earth neutral sheet region, *J. Geophys. Res.*, *97*, 1461, 1992.

Mandelbrot, B., *Fractals: Form, Chance and Dimension*, W. H. Freeman, New York, 1977.

McPherron, R. L., C. T. Russell, and M. P. Aubry, Satellite studies of magnetospheric substorms on August 15, 1968, 9, Phenomenological model for substorms, *J. Geophys. Res.*, *78*, 3131, 1973.

Ohtani, S., and T. Tamao, Does the ballooning instability trigger substorms in the near-Earth tail?, *J. Geophys. Res.*, *98*, 19,369, 1993.

Ohtani, S., S. Kokubun, R. C. Elphic, and C. T. Russell, Field-aligned current signatures in the near-tail region, 1, ISEE observations in the plasma sheet boundary layer, *J. Geophys. Res.*, *93*, 9709, 1988.

Ohtani, S., K. Takahashi, L. J. Zanetti, T. A. Potemra, R. W. McEntire, and T. Iijima, Tail current disruption in the geosynchronous region, in *Magnetospheric Substorms*, *Geophys. Monogr. Ser.*, vol. 64, edited by J. R. Kan, T. A. Potemra, S. Kokubun, and T. Iijima, pp. 131–137, AGU, Washington, D. C., 1991.

Ohtani, S., S. Kokubun, and C. T. Russell, Radial expansion of the tail current disruption during substorms: A new approach to the substorm onset region, *J. Geophys. Res.*, *97*, 3129, 1992.

Ohtani, S., et. al., A multisatellite study of a pseudo-substorm onset in the near-Earth magnetotail, *J. Geophys. Res.*, *98*, 19,355, 1993.

Osborne, A. R., and A. Provenzale, Finite correlation dimension for stochastic systems with power-low spectra, *Physica D*, *35*, 357–381, 1989.

Pellat, R., F. V. Coroniti, and P. L. Pritchett, Does ion tearing exist?, *Geophys. Res. Lett.*, *18*, 143, 1991.

Potemra, T. A., L. J. Zanetti, and M. H. Acuna, The AMPTE/CCE magnetic field experiment, *IEEE Trans. Geosci. Remote Sens.*, *GE-23*(3), 246–249, 1985.

Pulkkinen, T. I., D. N. Baker, R. J. Pellinen, J. Büchner, H. E. J. Koskinen, R. E. Lopez, R. L. Dyson, and L. A. Frank, Particle scattering and current sheet stability in the geomagnetic tail during the substorm growth phase, *J. Geophys. Res.*, *97*, 19,283, 1992.

Roux, A., S. Perraut, P. Robert, A. Morane, A. Pedersen, A. Korth, G. Kremser, B. Aparicio, D. Rodgers, and R. Pellinen, Plasma sheet instability related to the westward traveling surge, *J. Geophys. Res.*, *96*, 17,695, 1991.

Schindler, K., A theory of the substorm mechanism, *J. Geophys. Res.*, *79*, 2803, 1974.

Smith, R. A., C. K. Goertz, and W. Grossmann, Thermal catastrophe in the plasma sheet boundary layer, *Geophys. Res. Lett.*, *13*, 1380, 1986.

Takahashi, K., L. J. Zanetti, R. E. Lopez, R. W. McEntire, T. A. Potemra, and K. Yumoto, Disruption of the magnetotail current sheet observed by AMPTE CCE, *Geophys. Res. Lett.*, *14*, 1019, 1987.

Theiler, J., Some comments on the correlation dimension of $1/f^{\alpha}$ noise, *Phys. Lett. A*, *155*, 480–493, 1991.

Yamamoto, Y., and R. L. Hughson, Extracting fractal components from time series, *Physica D*, *68*, 250–264, 1993.

T. Higuchi, The Institute of Statistical Mathematics, Tokyo 106, Japan. (e-mail: higuchi@sunstar.ism.ac.jp)

A. T. Y. Lui and S. Ohtani, Applied Physics Laboratory, Johns Hopkins University, Johns Hopkins Road, Laurel, MD 20723-6099. (e-mail: lui@jhuapl.edu; ohtani@jhuapl.edu)

K. Takahashi, Solar Terrestrial Environment Laboratory, Nagoya University, Toyokawa 442, Japan. (e-mail: kazue@stelab.nagoya-u.ac.jp)

(Received December 6, 1994; revised March 2, 1995; accepted March 16, 1995.)